This is a repository copy of *Phosphorus availability influences disease-suppressive soil microbiome through plant-microbe interactions*.

Article:

RESEARCH

Phosphorus availability influences disease-suppressive soil microbiome through plant-microbe interactions

Yifan Cao[1†], Zongzhuan Shen[1*†], Na Zhang[1], Xuhui Deng[1], Linda S. Thomashow[2], Ian Lidbury[3], Hongjun Liu[1], Rong Li[1*], Qirong Shen[1] and George A. Kowalchuk[4]

Abstract

Background Soil nutrient status and soil-borne diseases are pivotal factors impacting modern intensive agricultural production. The interplay among plants, soil microbiome, and nutrient regimes in agroecosystems is essential for developing effective disease management. However, the influence of nutrient availability on soil-borne disease suppression and associated plant-microbe interactions remains to be fully explored. This study aims to elucidate the mechanistic understanding of nutrient impacts on disease suppression, using phosphorous as a target nutrient.

Results A 6-year field trial involving monocropping of tomatoes with varied fertilizer manipulations demonstrated that phosphorus availability is a key factor driving the control of bacterial wilt disease caused by *Ralstonia solanacearum*. Subsequent greenhouse experiments were then conducted to delve into the underlying mechanisms of this phenomenon by varying phosphorus availability for tomatoes challenged with the pathogen. Results showed that the alleviation of phosphorus stress promoted the disease-suppressive capacity of the rhizosphere microbiome, but not that of the bulk soil microbiome. This appears to be an extension of the plant trade-off between investment in disease defense mechanisms versus phosphorus acquisition. Adequate phosphorus levels were associated with elevated secretion of root metabolites such as L-tryptophan, methoxyindoleacetic acid, O-phosphorylethanolamine, or mangiferin, increasing the relative density of microbial biocontrol populations such as *Chryseobacterium* in the rhizosphere. On the other hand, phosphorus deficiency triggered an alternate defense strategy, via root metabolites like blumenol A or quercetin to form symbiosis with arbuscular mycorrhizal fungi, which facilitated phosphorus acquisition as well.

Conclusion Overall, our study shows how phosphorus availability can influence the disease suppression capability of the soil microbiome through plant-microbial interactions. These findings highlight the importance of optimizing nutrient regimes to enhance disease suppression, facilitating targeted crop management and boosting agricultural productivity.

Keywords Phosphorus, Soil-borne disease suppression, Phosphorus-defense trade-off, Soil microbiome, Plant-microbe interaction, Rhizosphere

---

†Yifan Cao and Zongzhuan Shen contributed equally to this work.

*Correspondence:
Zongzhuan Shen
shenzongz@njau.edu.cn
Rong Li
lirong@njau.edu.cn
Full list of author information is available at the end of the article

Background

Crop loss to soil-borne disease poses a persistent challenge to modern intensive agricultural systems [1]. Effective control of soil-borne disease outbreaks relies on two crucial factors: activating plant immunity and inducing soil disease suppressiveness, wherein resident microbes mitigate disease incidence [2]. Emergent research has also emphasized a critical role of soil nutrient status in shaping these two factors [3]. Thus, understanding the interplay between plants, soil microbiota, and nutrient regimes in diverse agro-ecosystems represents an urgent research priority for developing effective disease management and sustainable crop production.

Nutrient availability is a major constraint on terrestrial primary productivity [4]. Among plant nutrients, phosphorus, more specifically bioavailable orthophosphate, is frequently limited in soils due to fixation into insoluble complexes and intensive agriculture [5]. As phosphorus participates in diverse biochemical processes, acquisition of this important, but limited, nutrient affects numerous plant traits, as well as crop yields [5]. Recent research has examined the role of phosphate availability in plant defense. For example, it was proposed that production of fine root traits enabling efficient phosphate acquisition can lead to an increased susceptibility to soil-borne pathogens [4]. In *Arabidopsis thaliana*, the master transcriptional regulators responsible for the phosphate stress response directly inhibit the plant immunity response [6]. Since soil-borne disease control is a comprehensive system dependent on plant innate immunity and the composition of the soil microbiota [7], understanding soil disease suppressiveness is another crucial aspect to consider.

It is widely known that soil disease suppressiveness, especially general suppressiveness, is determined by the interaction between microorganisms and environment [8]. Soil microorganisms play pivotal roles in promoting plant health through various direct and indirect mechanisms, including activation of plant defense responses, antibiotic production against phytopathogens, and improvement of nutrient availability [9–11]. Soil chemical properties, such as soil pH and nutrient concentrations, are key factors influencing microbial communities in bulk and rhizosphere soils [12, 13]. Recently, the concept of soil nutrient characteristics indirectly contributing to soil disease suppression via the manipulation of microbial communities has gained attention [14], especially in relation to phosphate availability. For instance, high phosphate availability has been found to significantly contribute to soil disease suppression by stimulating biocontrol agents, such as *Pseudomonas* spp. [15]. However, there are also reports indicating that high phosphate availability can increase pathogen abundance

and the reduce of beneficial microbial populations in the rhizosphere [16]. Thus, the precise impact of phosphorus status on disease suppressiveness mediated by the soil microbiota remains uncertain.

Understanding the mechanism by which soil phosphorus status influences soil microbial assembly and functionality in disease suppression represents a knowledge gap that currently impedes our ability to predict and steer disease suppression in agricultural systems. To address this knowledge gap, we collected data from a 6-year tomato monoculture field trial that included four fertilizer treatments. Soil nutrient properties and bacterial wilt disease incidences caused by *Ralstonia solanacearum* were used to examine the relationship between phosphorus availability and disease incidence. We then sought to delve deeper into potential links between phosphorous availability and soil disease suppression by conducting targeted pot experiments focusing on the impact of a gradient phosphorus stress, mediated by phosphate availability, on soil microbial function related to disease suppression. The model system employed the commonly used tomato cultivar 'Micro-Tom' (Solanaceae family) and the soil-borne pathogen *R. solanacearum* [17]. We assessed the disease suppressive potential of the soil microbiome based on the abundance of microbial functional genes involved in the biosynthesis of nonribosomal peptide synthases (NRPS), polyketide synthases (PKS), hydrogen cyanide (HCN), and 2,4-diacetylphloroglucinol (2,4-DAPG) production [18–22]. NRPS and PKS are major enzyme families responsible for the production of bioactive microbial metabolites, including many antibiotics and antifungals, and their corresponding genes have been identified as key contributing factors towards suppressive soils [10, 23, 24]. We also considered genes related to the production of 2,4-diacetylphloroglucinol (*phlD*) and hydrogen cyanide (*hcnAB*), as these compounds have been demonstrated to inhibit *R. solanacearum* in tomato bacterial wilt [25]. Using these functional markers of secondary metabolite production, we examined several mechanisms of microbiota-mediated disease suppression.

In addition, 16S rRNA and ITS amplicon sequencing were used to characterize the bacterial and fungal communities in bulk and rhizosphere soil compartments. Transcriptomic and widely targeted metabolomic analyses of tomato roots were used to determine how plant performance affects the rhizosphere microbiome. Specific microbes affected by phosphate availability were also isolated, and we investigated their inhibitory capacity against pathogens in the presence of the identified key root metabolites. In this study, we aimed to address three key questions: (1) Does soil phosphate availability influence the occurrence of soil-borne disease? (2) How

do soil microbial functions associated with disease suppression respond to varying levels of soil phosphate availability? and (3) What role do plants play in this dynamic? Our study aims to elucidate the influence of soil phosphorus on soil disease suppression capacity, offering valuable insights into the relationship between soil nutrient status and soil-borne disease suppression, as well as associated plant-microbe interactions.

Methods

The long-term field trial of tomato afflicted by bacterial wilt

Our long-term field trial was conducted at the Institute of Vegetables and Flowers, Nanjing, Jiangsu Province (32°02′ N, 118°50′ E), situated in a typical subtropical monsoon climate. The region experiences an average annual temperature of approximately 15.4 °C and an average annual precipitation of about 1106 mm. The soil is developed from a loess parent material with a clay loam texture and is classified as moisture soil. The trial was carried out in a greenhouse previously dedicated to the cultivation of tomatoes (*Solanum lycopersicum* Mill. cv. Shijihongguan) afflicted by bacterial wilt caused by *R. solanacearum*. Four distinct fertilization treatments were implemented: (1) CK — no fertilizer applied, (2) CF — application of chemical fertilizer, (3) OF — application of organic fertilizer, and (4) BF — application of bio-organic fertilizer. The latter three treatments were adjusted to an equivalent amount of nitrogen, phosphorus, and potassium using chemical fertilizer.

The experiment employed a completely random block design, with three replication plots designated for each treatment a total of 12 plots. Each plot covered an area of approximately 8 m^2, accommodating 40 tomato plants. Two tomato planting seasons occurred annually from March 2013 to July 2019. The spring season was from March to June, while the autumn season was from August to November. Over the course of 13 consecutive seasons, only the spring seasons were sampled, with the first season excluded due to the absence of bacterial wilt outbreaks across all four treatments. Approximately 2-month post-transplantation of tomato seedlings to the field, the recording of disease incidence in each plot commenced. Plants displaying typical symptoms of bacterial wilt were identified as diseased and recorded until the end of the tomato harvest. Disease incidence was calculated as the number of diseased tomato plants in a plot divided by the total number of tomato plants in that plot. Soil samples were collected at the time of tomato harvest, with a portion sieved through a 20-mm mesh for nutrient property determination. Tomatoes were cultivated for 3 months per season, adhering to standard agronomic management practices, except for variations in the fertilizer managements.

Basic information of tested soil, tomato cultivar, and pathogen in pot experiment

The soil with low phosphate availability used in our pot experiments was collected from a poplar plantation located in Baoying County, Yangzhou, Jiangsu Province, China (119° 36′E, 33° 21′N). The collected soil represents a typical fluvo-aquic soil, with the following characteristics: organic matter content of 8.75 g kg^{-1}, available phosphorus content of 10 mg kg^{-1}, total nitrogen content of 0.49 g kg^{-1}, and available potassium content of 223 mg kg^{-1}.

The tomato cultivar 'Micro-Tom' (*Solanum lycopersicum* L.) was selected for this study. Tomato seeds were surface sterilized in 70% ethanol for 1 min and then soaked in 1% NaClO for 10 min, after which they were rinsed five times with sterile water. Tomato seeds were germinated on moist filter paper in petri dishes for three days at 30 °C. Budded seeds were sown in sterilized commercial nursery substrate (Xingnong Substrate Technology Co., Ltd., Jiangsu, China) and then incubated to the two-leaf stage before being transplanted into pots. Plant growth conditions consisted of 14-h light and 10-h dark at 28 °C.

R. solanacearum strain QL-Rs1115 (GenBank accession GU390462) was used as a model soil-borne pathogen. The stain was isolated and stored in our laboratory. The pathogen suspension was prepared according to a previous method [26]. *R. solanacearum* was grown in Nutrient Broth (NB) medium (glucose 10.0 g L^{-1}, peptone 5.0 g L^{-1}, yeast extract 0.5 g L^{-1}, beef extract 3.0 g L^{-1}) at 30 °C for 2 days with shaking at 170 rpm. The culture was then centrifuged at 4000 rpm for 8 min, and the resulting cell pellet was resuspended in sterile water. The final density of the prepared *R. solanacearum* inoculation was 1×10^8 colony-forming units (CFU) per ml.

Greenhouse experiment design examining soil microbial functions in relation to disease suppression

We aimed to investigate how soil microbial functions potentially related to disease suppression responded to varying levels of phosphorus. A pot experiment was conducted in the greenhouse of Nanjing Agricultural University, Nanjing, China (118.847 °E, 32.036 °N). The experiment included six treatments and a control. The six treatments were as follows: (1) AP, soil amended with calcium superphosphate as a source of relatively available phosphorus; (2) UP, soil amended with calcium phosphate as a source of relatively unavailable phosphorus; (3) −P: soil without application of external phosphorus supply; (4) AP+RS, AP with pathogen inoculation; (5) UP+RS, UP with pathogen inoculation; and (6) −P+RS,

−P with pathogen inoculation. The control (CK) treatment consisted of soil without any fertilization or pathogen inoculation. The total phosphorus input was kept consistent across the AP, UP, AP+RS, and UP+RS treatments. Each treatment had six replicates, with each replicate containing three tomato seedlings in three pots filled with 500 g of the test soil. The pots were arranged using a completely randomized block design. The phosphorus stress gradient in the soil was created by the application of calcium superphosphate (AP, AP+RS), calcium phosphate (UP, UP+RS), and the absence of any phosphorus fertilizer (−P, −P+RS).

Urea and potassium sulfate were provided as nitrogen and potassium fertilizers in all treatments except the control (CK), and phosphorus fertilizers were applied according to the experimental design (Table S1). Prior to the second season, approximately half of the initial fertilizer amount was replenished to compensate for the nutrient loss after harvest. Tomato plants in the AP+RS, UP+RS, and −P+RS treatments were inoculated with *R. solanacearum* at a density of 1×10^7 CFU g^{-1} soil, 3 days after transplanting. The pathogen was subsequently added two additional times, once at the flowering stage and once at the fruiting stage. For treatments without pathogen inoculation, an equal volume of sterilized water was provided. The experiment was repeated twice. The first season started on October 22, 2020, and ended on January 13, 2021, and the second season started on March 21, 2021, and ended on June 12, 2021.

Soil sampling and DNA extraction

Soil sampling was conducted 80 days after tomato transplantation. Soils were collected from each pot at five different points and then combined to obtain a bulk soil sample. Soil loosely attached to the plant roots was removed by manually shaking, and the soil that remained tightly adhered to the roots was considered the rhizosphere compartment. The roots were submerged in sterilized water and shaken at 170 rpm for 30 min at 30 °C. The resulting soil suspension was centrifuged at 5000 rpm for 10 min to collect the rhizosphere soils. The rhizosphere soils from three plants within one replicate were combined to form a single sample ($n = 6$ in total). A portion of the bulk soil was air-dried for soil chemical property assessment. Soil samples were stored at −80 °C for subsequent microbial community analysis, with a portion of the rhizosphere soil was preserved in glycerol for the culture-dependent analysis. Soil genomic DNA was extracted from 0.3 g of soil using the DNeasy® PowerSoil® Kit (QIAGEN GmbH, Germany) following the manufacturer's instructions. DNA extracts

were quantified using a NanoDrop spectrophotometer (ND2000, Thermo Scientific, DE, USA).

Quantitative PCR of *R. solanacearum* and functional genes

The *R. solanacearum* abundance was determined by targeting the *fliC* gene [27]. Microbial genes related to disease suppression, including NRPS, PKS, *hcnAB*, and *phlD*, were determined with the primer sets A3F/A7R [28], KS2F/KS2 [29], PM2/PM7-26R [21], and BPF2/BPR4 [21], respectively. For relative quantification, the 16S ribosomal RNA gene, as amplified by the primer pair of F515/R907, was used as a reference gene as previously described [30]. The detailed information describing the primers used is given in Table S2. Quantitative gene abundance was defined as the proportion of target gene abundance to 16S rRNA gene abundance. Mathematical model ∆∆Ct was used in relative quantification data processing [31].

All qPCR amplifications were performed using a QuantStudio™ 6 Flex Real-Time PCR System (Applied Biosystems, USA). PCR reaction for each sample (10 µL) contained 5 µL of TB Green™ Premix Ex Taq™ (RR420A, TaKaRa), 0.2 µL of each primer (10 µM), 1-µL DNA template, 0.1-µL bovine serum albumin (10 µg $µL^{-1}$), and 3.5-µL ddH$_2$O. All qPCR amplifications were performed with an initial denaturation at 95 °C for 2 min, then 40 cycles of denaturation at 95 °C for 30 s, annealing at 58 °C for 30 s, and extension at 72 °C for 30 s. All analyses were performed in duplicate, resulting in a total 12 parallel reactions for each treatment. The results were expressed as log2 fold change values (log FC) relative to the CK treatment.

16S rRNA gene and ITS amplicon sequencing and data processing

Bacterial and fungal sequencing libraries were amplified using the V4–V5 region of bacterial 16S rRNA gene (515F/907R) and the fungal ITS region (ITS5-1737F/ITS2-2043R) (Table S3). PCR utilized the following thermocycling program: 5 min at 94 °C for initialization, 30 cycles of 30-s denaturation at 94 °C, 30-s annealing at 52 °C, and 30-s extension at 72 °C. The constructed libraries were sequenced using an Illumina Nova6000 platform (Guangdong Magigene Biotechnology Co., Ltd. Guangzhou, China).

Raw sequences were processed according to the procedure of USEARCH v. 9.1.1354, using a UNOISE2 algorithm to obtain zOTU table. The taxonomy predictions were made using the "sintax" command with a bootstrap confidence threshold of 0.6, based on the silva_16s_v123 and UNITE 8.2 databases [32–34].

Soil nutrient contents determination

Soil nutrient contents, such as organic matter, total nitrogen, available phosphorus, and available potassium, were quantified using established methods [35, 36]. In brief, soil organic matter content was determined using the potassium dichromate-volumetric method. Total nitrogen content was measured using an element analyzer. Available potassium was assessed by extraction with ammonium acetate solution and quantification using a flame photometer. Available phosphorus was assessed by extraction with sodium bicarbonate solution and the molybdenum antimony anti-colorimetric method. All results are given in Fig. S1 and Table S4.

Greenhouse experiment for tomato root transcriptome and metabolome analyses

We aimed to investigate the impact of root transcription and root exudates on microbial function related to disease suppression in the rhizosphere under different phosphorus levels. To this end, a pot experiment similar to the one described above was conducted, but the soil was changed to a mixture of soil and sand (weight 1:1) to facilitate root sampling. The experiment consisted of three replicates with two tomato seedlings in each replicate. This experiment was carried out from September 15 to November 28, 2022. The tomato roots were sampled by pooling two plants into one replicate as follows. Briefly, tomato plants were carefully pulled out and shaken gently to remove adhering soil. Then they were shaken in sterile water for 10 s to remove rhizosphere soil, followed by a quick separation of the aboveground part and root by sterile scissors on a tinfoil platform that had been wiped with alcohol. The roots were cut into 3-cm pieces, approximately 5 g of which were placed into a 15-ml centrifuge tube and immediately frozen in liquid nitrogen. This process was quickly completed, within 10 min, for each sample.

Plant transcriptome sequencing and widely targeted metabolome analyses were conducted by Metware Biotechnology Co., Ltd. (Wuhan, China). For transcriptome analysis, total RNA was extracted, quantified, and qualified. Subsequently, 1 μg of RNA per sample was used for library preparation using the NEBNext® UltraTM RNA Library Prep Kit for Illumina® (NEB, USA) according to the manufacturer's instructions. The prepared libraries were then sequenced on an Illumina platform. Quality control was performed using fastp v0.19.3, and clean reads were aligned to the reference genome ftp://ftp.ensemblgenomes.org/pub/plants/release-52/fasta/solanum_lycopersicum/dna/ using HISAT v2.1.0. New transcript predictions were made using StringTie v1.3.4d, and gene expression levels were estimated using TPM (transcripts per million). The genes were annotated using the Kyoto Encyclopedia of Genes and Genomes (KEGG) and Gene Ontology (GO) databases.

For metabolome analysis, freeze-dried root samples were powdered, and 50 mg of the powder was used for metabolite extraction. The extracted samples were analyzed using an UPLC-ESI-MS/MS system (UPLC, ExionLC™ AD, https://sciex.com.cn/; MS, Applied Biosystems 6500 QTRAP, https://sciex.com.cn/). Metabolite identification was performed using the MWDB (Metware database) provided by Metware Biotechnology Co., Ltd. (Wuhan, China).

Isolation of key microorganisms from the rhizosphere and resistance testing against pathogens in the presence of root metabolites

We isolated and identified potential disease-suppressive microorganisms influenced by phosphorus status. Frozen rhizosphere soils in 30% glycerol from the AP+RS treatment were recovered from soil suspensions and used to make serial diluted and plated on modified R2A culture medium, following the method described by Nishioka et al. [37]. To avoid the formation of compounds that may be inhibitory to some sensitive bacteria, phosphate compounds were autoclaved separately from the agar, with the culture medium being prepared as two separate solutions. Solution A (500 ml) was prepared using yeast extract 0.5 g, tryptone 0.25 g, peptone 0.75 g, starch 0.5 g, glucose 0.5 g, agar 15 g, and deionized water 500 ml. Solution B (500 ml) was prepared using K_2HPO_4 0.3 g, $MgSO_4 \cdot 7H_2O$ 0.0462 g, sodium pyruvate 0.3 g, and deionized water (500 ml). Solutions A and B were autoclaved separately and mixed together before use. After incubating the plates at 28 °C for 1 week, a total of 133 isolates were randomly selected and purified. The isolates were taxonomically classified through the NCBI pipeline, based on their 16S rRNA gene sequences after the colony PCR method with primers 27F and 1492R [38]. One-hundred twenty-six isolates were identified in total (Table S5).

To investigate the pathogen inhibitory capacity of key isolates in the absence or presence of the key root exudates identified from the root metabolome analyses, co-culture experiments with the pathogen *R. solanacearum* (RS) were conducted. The four treatments were as follows: (1) RS + key microbe + exudate, (2) RS + key microbe, (3) RS + exudate, and (4) RS. The fluorescence intensity of *R. solanacearum* was determined on BioTek Synergy H1 (excitation: 561 nm, emission: 600 nm). The system consisted of 100-μL 1/2 NB culture medium, 10 μL of a RS suspension (OD_{600} (optical density) = 0.1), 10 μL of a suspension of the key microbe (OD_{600} = 0.1), and 30 μL of a root exudate solution. Three concentration levels 10 mmol L^{-1}, 2 mmol L^{-1}, and 0.4 mmol L^{-1} were tested for root exudates

that were soluble in water, such as L-tryptophan, O-phosphorylethanolamine, and acetoxyacetic acid [39–41]. One concentration level (0.4 mmol L^{-1}) was tested for exudates soluble in 4% DMSO, but not in water, such as mangiferin, methoxyindoleacetic acid, xanthosine, and phenylpyruvic acid. This was because that higher exudate concentrations would have required higher DMSO concentrations, which would have inhibited bacterial growth. In total, there were 75 treatments with 6 replicates of each treatment. Cultures were grown in a black microtiter plate (200 μL well^{-1}) at 30 °C with agitation at 170 rpm. The pathogen's fluorescence intensity was recorded every 12 h for 96 h. Additionally, the effect of key exudates on key microbes was tested on BioTek Synergy H1 (OD_{600}) with the same set of concentrations as described above.

Statistical analyses and visualization

Statistical analyses were carried out using R (version 4.0.4) software. To investigate the impact of soil nutrient properties on disease incidence, we employed unary linear regression, standardized multiple linear regression, and the random forest method. These analyses utilized the "randomForest," "rfPermute" packages, "lm," and "scale" functions. Microbial community analysis was conducted using the "Vegan" package, which included principal coordinates analysis (PCoA) based on Bray-Curtis distance, also for the transcriptome and metabolome analysis of plant root. The Mantel test and PERMANOVA test were used to evaluate the effects of phosphorus stress and pathogen inoculation on microbial composition. For different data analysis, the Scheirer-Ray-Hare test, Wilcoxon test, and Kruskal Wallis test were applied, using the "rcompanion," "stats," and "agricolae" packages. Spearman correlations were computed using the "cor.test" command. Weighted gene co-expression network analysis (WGCNA) was performed using genes associated with pathogen response and phosphate starvation in the roots, along with all metabolites. The "WGCNA" package was utilized, and network modules were defined with a minimum of 200 members per module. Data processing involved the following packages: "reshape2," "xlsx," "agricolae," "dplyr," and "rstatix." Cladogram construction was performed using the "microbiomeViz," "ggtree," "treeio," "ggtreeExtra," "ggnewscale," and "ggstar" packages. Other graphical representations were generated using the "ggplot2," "ggbeeswarm," "RColor-Brewer," "corrplot," "pheatmap," and "circlize" packages.

Results

The influence of soil nutrient content on bacterial wilt incidence

The 6-year-old tomato monoculture field trial was established to examine the relationship between a range of soil nutrient properties and the incidences of bacterial wilt disease (DI) caused by *R. solanacearum* (Fig. 1A). Multiple linear regression, focusing on standardized nutrient properties and DI, revealed soil available phosphorus (AVP) as the primary influential factor on disease incidence (estimate = −0.55, P = 2.65E-05), followed by soil organic matter (SOM) content (estimate = −0.23, P = 0.084) (Fig. 1B). The resulting model had an adjusted R-squared value of 0.3704 and a P-value of 3.88E-07. Consistently, the outcomes of the random forest prediction indicated AVP as the most significant factor influencing DI, followed by SOM, total nitrogen, and available potassium, explaining 46.04% of the variance (Fig. 1C). Unary linear regression clearly showed that the increase of AVP was significantly linked to reduced DI (Fig. 1D), and this effect was more pronounced compared to other nutrient properties (Fig. S1B). Detailed data on soil nutrient contents and DI are given in Fig. S1A. The consistent findings across these three methods strongly support the premise that elevating soil phosphorus status represents the primary nutrient factor related to disease suppression.

Effects of phosphorus on microbial functions related to disease suppression in bulk and rhizosphere soils

Based on our initial field trial, we next established a controlled pot experiment, whereby we manipulated a naturally low phosphorus soil (available phosphorus = 10.34 mg kg^{-1}), generating a phosphorus stress gradient (Fig. 1E; Fig. S2A). After fertilization, the soil available phosphorus contents averaged across all time points were 18 mg kg^{-1} in the AP treatment, 12 mg kg^{-1} in the UP treatment, 6 mg kg^{-1} in the −P treatment, and 7 mg kg^{-1} in the CK control (Table S4). Each phosphorus treatment was subjected to inoculation of the pathogen *R. solanacearum* at a density of 1 × 10^7 CFU g^{-1} soil (Fig. S2B), showing a consistent and effective pathogen inoculation across all levels of phosphorus stress.

Next, we analyzed genes responsible for encoding disease suppression in bulk (Fig. 2 A, B, and C) and rhizosphere (Fig. 2 D, E, and F) soils using quantitative PCR approaches. The *phlD* gene was not detected and has therefore been excluded from further discussion. In both bulk and rhizosphere soils, strong positive correlations were observed for genes encoding NRPS, PKS enzymes, and *hcnAB* (Fig. 2 C and F). The data from the three highly correlated genes were pooled together to simplify downstream analyses, with detailed results of individual genes given in Fig. S3. Scheirer-Ray-Hare test results demonstrated significant influences of phosphorus stress and pathogen inoculation on disease-suppressive genes in general. In bulk soil samples, the abundance of disease-suppressive genes increased significantly with heightened phosphorus stress when under pathogen
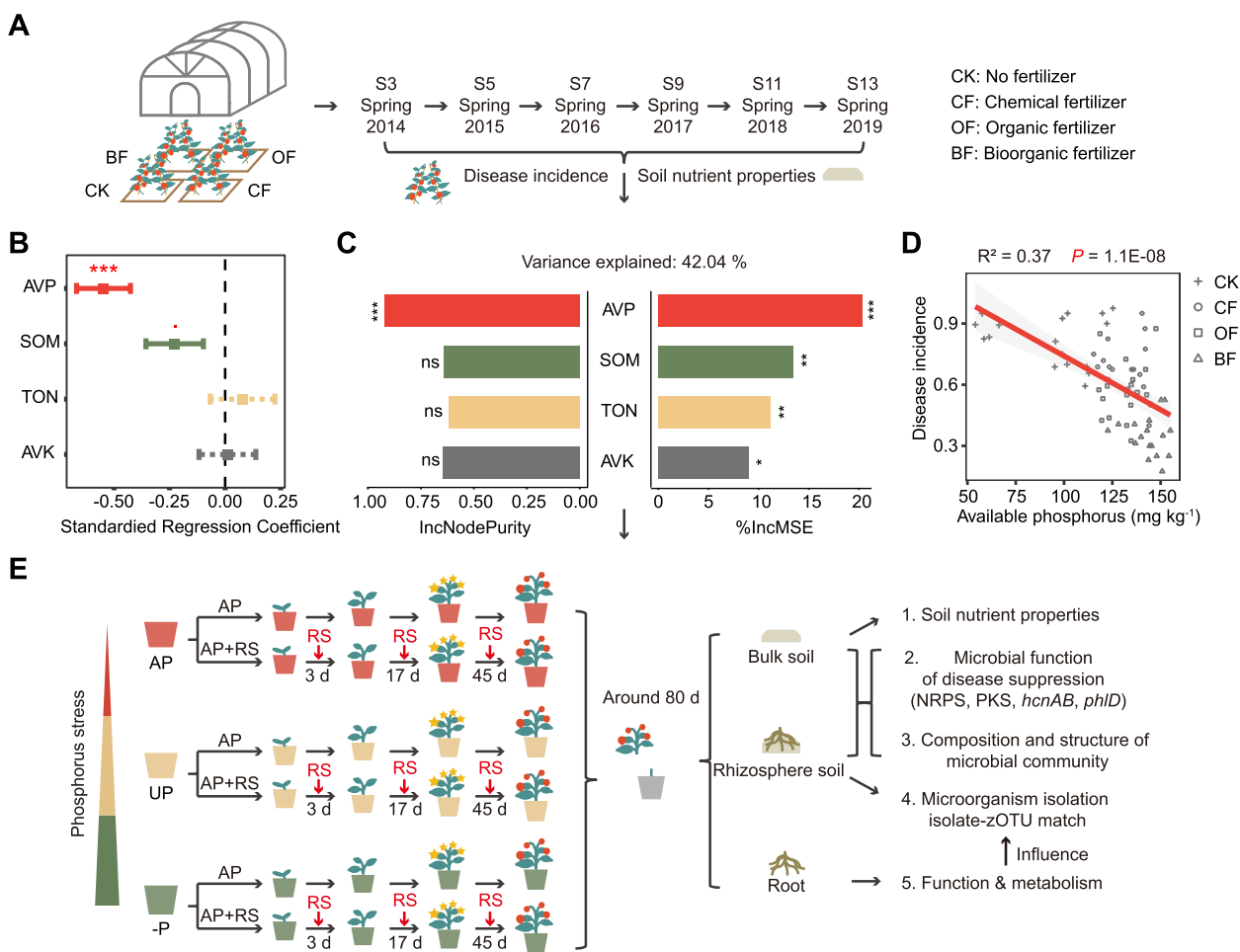
Fig. 1 Experimental design and the influence of soil nutrient properties on disease incidence. **A** Schematic of the field trial design, with each treatment comprising three replication plots, each containing 40 tomato plants. **B** The relationship between standardized nutrient properties and disease incidence (DI) caused by pathogen *R. solanacearum*, using multiple linear regression analysis. **C** The influence of soil nutrient properties on DI, predicted by random forest method. **D** Relationship between soil available phosphorus and DI, using unary linear regression analysis. **E** Schematic of the pot experiment design. Six replicates, each containing three tomato plants, were employed during seasons 1 (2020 October 22-2021 January 13) and 2 (2021 March 21-2021 June 12). Three replicates, each containing two tomato plants, were employed during season 3 (2022 September 15-2022 November 28). Seasons 1 and 2 corresponded to trials 1 through 4, while season 3 was dedicated to the 5th trial. All treatments depicted in this figure received equivalent nitrogen and potassium fertilization. The CK control, without any fertilization or pathogen inoculation, is not shown. Treatments include AP, soil applied with calcium superphosphate as relatively available phosphorus; UP, soil applied with calcium phosphate as relatively unavailable phosphorus with equivalent amount phosphorus to AP treatment; −P, soil with no phosphorus supply. Phosphorus stress gradually increased in the order of AP, UP, and −P. +RS groups were inoculated with pathogen at 1×10^7 colony-forming units g^{-1} soil. RS denotes *R. solanacearum*; P denotes phosphorus. Significance levels are denoted as follows: "ns," not significant, "."$P < 0.1$, "*"$P < 0.05$, "**"$P < 0.01$, and "***"$P < 0.001$

amendment ($r = 0.23$, $P = 0.015$) (Fig. 2A), with genes encoding NRPS and PKS enzymes contributing significantly to this effect (Fig. 2B). However, the opposite effect was observed in the rhizosphere. Here, alleviation from phosphorus stress resulted in a significant increase of disease-suppressive genes upon pathogen inoculation ($r = -0.30$, $P = 0.0013$) (Fig. 2D), with genes encoding NRPS and *hcnAB* contributing more prominently

to this effect (Fig. 2E). Furthermore, in the rhizosphere, disease-suppressive genes were significantly increased by pathogen inoculation in the AP and UP treatments, with a more pronounced effect observed in the AP (Fig. 2D). Overall, the potential disease-suppressive ability of the rhizosphere microbiome was enhanced by the alleviation of phosphorus stress and inoculation of the pathogen, a pattern that was in contrast to that observed in bulk soil.
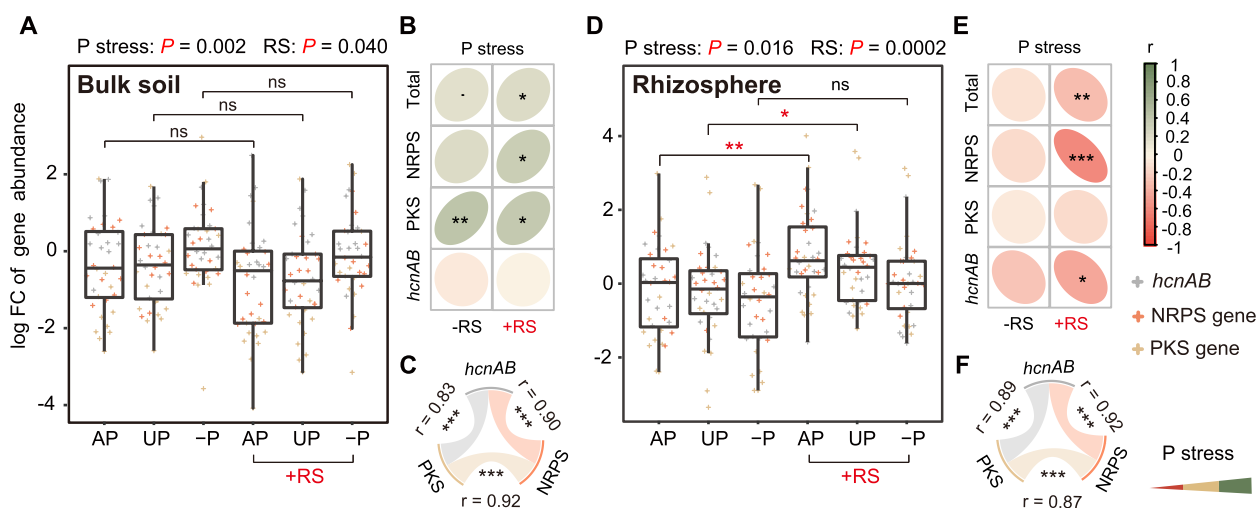
Fig. 2 Contrasting responses of microbial disease-suppressive genes to phosphorus stress in bulk and rhizosphere soils. Results from the quantitative PCR analysis were pooled for seasons 1 and 2. Phosphorus stress gradually increased in the order of AP, UP, and −P because of different fertilizer treatments. **A** and **D** Fold changes of disease-suppressive genes in bulk and rhizosphere soils compared to the CK group. Scheirer-Ray-Hare test and Wilcoxon test were conducted. **B** and **E** Spearman correlations between the disease-suppressive genes and phosphorus stress in bulk and rhizosphere soils, with or without pathogen inoculation. Colors and circle shapes represent the correlation coefficient. **C** and **F** Spearman correlations within the three disease-suppressive genes of NRPS, PKS, and *hcnAB* in bulk and rhizosphere soils. +RS denotes *R. solanacearum* inoculation; P denotes phosphorus. Significance levels are denoted as follows: "ns," not significant, "."*P* < 0.1, "*"*P* < 0.05, "**"*P* < 0.01, and "***"*P* < 0.001
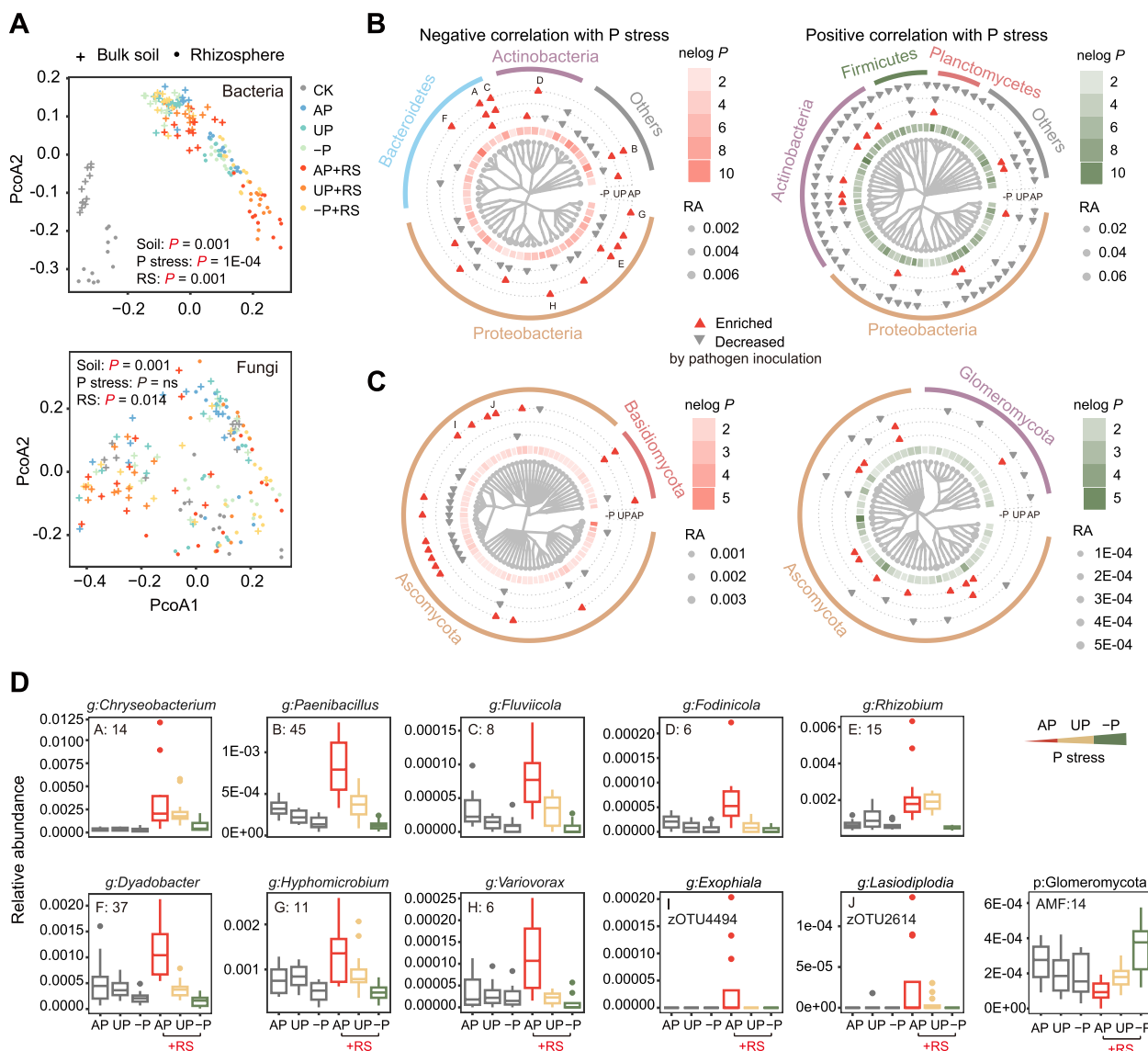
Impacts of phosphorus and the pathogen on the soil microbiome

Principal coordinate analysis (PCoA) was used to examine the influence of phosphorus stress, pathogen inoculation, and soil compartment (rhizosphere or bulk soils) on microbial community structure. Both bacterial and fungal communities exhibited significant responses to both the pathogen and soil compartment, with the bacterial community showing a more pronounced response ($P = 0.001$) compared to the fungal community ($P = 0.014$) with respect to impact of the pathogen (Fig. 3A). While the bacterial community was significantly altered by phosphorus availability ($P = 1E-04$), phosphorus availability did not significantly impact fungal communities ($P = 0.12$) (Fig. 3A).

Spearman correlations were conducted to assess the relationship between phosphorus stress and zOTU relative abundance in both soil compartments in the presence of the pathogen. Significantly correlated zOTUs ($P < 0.05$) are depicted in Fig. S4, identified up to the phylum level. Subsequently, among these zOTUs, those successfully identified to the genus level were extracted for further analysis. In bulk soil, heightened phosphorus stress was associated with fluctuations in the abundance of numerous bacterial taxa, for example, the *Blastococcus* (Fig. S5).

In the rhizosphere, numerous bacterial zOTUs from various genera were significantly correlated with phosphorus stress ($P < 0.05$, Fig. 3B), with many also significantly

($P < 0.05$) increasing or decreasing in respond to pathogen inoculation. In addition, several fungal zOTUs were also significantly altered by phosphorus availability (Fig. 3C). Specifically, the alleviation of phosphorus stress promoted bacterial zOTUs in the phylum Bacteroidetes, while phosphorus stress condition promoted zOTUs in the phyla Firmicutes and Planctomycetes (Fig. 3B). Similarly, the alleviation of phosphorus stress favored fungal zOTUs in the phylum Basidiomycota, whereas phosphorus stress condition promoted zOTUs in the phylum Glomeromycota (Fig. 3C). A more detailed classification of these microbial taxa can be found in Fig. S6 (for bacteria) and Fig. S7 (for fungi). Among these, many zOTUs were deemed to be potential disease-suppressive taxa, illustrated by their stimulated relative abundance in the presence of the pathogen, which was most pronounced under the alleviation of phosphorus stress (Fig. 3D and Table S6). Notably, a group of 14 zOTUs in the genus *Chryseobacterium* was stimulated by pathogen inoculation across all three levels of phosphorus stress (−P: $P = 0.0068$, UP: $P < 0.0019$, and AP: $P = 0.000022$), with further promotion observed with phosphorus stress alleviation ($P = 0.00067$, $r = −0.54$). Other noteworthy taxa included 45 zOTUs of *Paenibacillus*, 8 zOTUs of *Fluviicola*, 6 zOTUs of *Fodinicola*, 15 zOTUs of *Rhizobium*, 37 zOTUs of *Dyadobacter*, 11 zOTUs of *Hyphomicrobium*, 6 zOTUs of *Variovorax*, and two fungal zOTUs of *Lasiodiplodia* and *Exohiala*. We also found that a group of 14 zOTUs in the phylum

Fig. 3 Impact of phosphorus and pathogen inoculation on soil microbiome. Phosphorus stress gradually increased in the order of AP, UP, and −P due to different fertilizer treatments. The +RS groups indicated treatments inoculated with the pathogen. **A** Principal coordinate analysis (PCoA) plot illustrating the Bray-Curtis distance of bacterial and fungal communities among various treatments. PERMANOVA test evaluated differences due to soil compartment and pathogen inoculation, while the Mantel test assessed the effect of phosphorus gradient. **B** Cladogram displaying bacterial zOTUs correlated to phosphorus stress pooled at the genus level in the rhizosphere (Spearman correlation, $P < 0.05$, each genus with at least six or more zOTUs). **C** Cladogram showing fungal zOTUs correlated to phosphorus stress in the rhizosphere (Spearman correlation, $P < 0.05$, each phylum with at least six or more zOTUs). The red and black triangles represent microbial taxa enriched or decreased by pathogen inoculation in the −P, UP, or AP groups using the Wilcoxon test ($P < 0.05$). The "nelogp" denotes the negative log-transformed P-value of the Spearman correlations between the microbial taxa and phosphorus stress. "RA" stands for relative abundance. The phylum classification is labelled around the cladogram. **D** The relative abundances of identified key microbial taxa responding to phosphorus stress and pathogen inoculation in rhizosphere soils. The numbers in boxplots in **A**, **B**, **C**, **D**, **E**, **F**, **G**, and **H** and for AMF correspond to the number of zOTUs included for the given taxon

Glomeromycota that decreased in response to the pathogen in AP ($P = 0.00020$) remained unchanged in UP ($P = 1$), and increased in −P ($P = 0.0083$), thus showing a significant increase with rising phosphorus stress in the presence of the pathogen (Fig. 2 C and D).

Potential disease-suppressive microbial taxa promoted by phosphorus are influenced by plant root function and root metabolites

PCoA plots revealed a significant influence of phosphorus stress on both plant root transcriptome ($P = 1E-04$)

and metabolome (P = 1E-04), but not statistically significantly for pathogen inoculation (P = 0.091, P = ns, Fig. 4A). Notably, a transcriptional shift in response to pathogen inoculation was more pronounced in the AP and UP treatments, compared to the −P. We first identified the 1111 pathogen-related genes and 139 phosphorus starvation genes based on the function annotation using KEGG and GO databases (Tables S7 and 8). Then as expected, in plant roots, these phosphorus starvation genes showed an increase with increasing phosphorus stress (+RS: P = 9.585E-05, r = 0.95; −RS: P = 9.585E-05, r = 0.95) (Fig. 4B). Importantly, pathogen-related genes were significantly upregulated by pathogen inoculation (P = 0.024), and they showed a significant reduction with increasing phosphorus stress (+RS: P = 0.0043, r = −0.84; −RS: P = 0.011, r = −0.79) (Fig. 4B). This suggests phosphorus stress is related to the reduced level of pathogen response regulon.

We constructed a WGCNA network to identify potential metabolites involved in phosphorus-affected plant defense to further explore their corresponding influence on rhizosphere microorganisms (Fig. 4C). The network was divided into several modules, each comprising at least 200 members, with the important modules identified and depicted in the heatmap (Fig. 4D). The module eigengenes of turquoise module increased with increasing phosphorus stress, whereas those of the yellow and blue modules increased with decreasing phosphorus stress (Fig. 4D). Additionally, several key metabolites were identified in the histogram (Fig. 4D). Acetoxyacetic acid (organic acids), L-tryptophan (amino acids and derivatives), O-phosphorylethanolamine (alkaloids), methoxyindoleacetic acid (alkaloids), mangiferin (flavonoids), phenylpyruvic acid (organic acids), and xanthosine (nucleotides and derivatives) were associated with the yellow and blue modules and were promoted by phosphorus supply (Fig. 4D), consistent with the trends observed in plant pathogen-related functions (Fig. 4B) and soil microbial disease-suppressive functions in the rhizosphere (Fig. 2D). Blumenol A and quercetin (flavonoids), present in the turquoise module, were promoted by phosphorus deficiency and also stimulated by the presence of the pathogen in the −P treatment (Fig. 4D). The detailed information of these metabolites is given in Table S9.

Next, we were able to recover isolates that corresponded to the key zOTUs that promoted by phosphorus supply and stimulated by pathogen inoculation (Figs. 3D and 5A). Four of these isolates were identified as *Chryseobacterium* (Y14 and Y35) (Fig. S8), *Dyadobacter* (Y33) (Fig. S9), and *Paenibacillus* (R16) (Fig. S10). Y33 and R16 were selected because they were the only *Dyadobacter* or *Paenibacillus* among our 126 isolates. For

Chryseobacterium, we recovered eight isolates that clearly separated into two different species based on phylogeny and morphology (Fig. S11). We selected one isolate from each of these species, Y14 and Y35, for the subsequent assay. The relative abundances of the zOTUs that are most related to the isolated key bacteria are given in Fig. S12. Pairwise co-culture growth experiments were conducted to individually assess capacity of these isolates to inhibit the growth of bacterial pathogen *R. solanacearum*, (Fig. 5B). In the absence of root metabolites, *Chryseobacterium* strains Y14 and Y35 showed significant inhibition of the pathogen, with Y35 being more inhibitory than Y14. *Paenibacillus* strain R16 showed no inhibition, and *Dyadobacter* strain Y33 even promoted pathogen growth, with significant results shown in Table S10.

We repeated these co-culture experiments, this time individually supplementing the identified root exudates into the growth medium at differing concentrations (Fig. 5C and Figs. S13 to 19). Root metabolite treatments influenced the degree of pathogen inhibition, in some cases even without the beneficial bacteria, for example, O-phosphorylethanolamine (Fig. 5C). *Chryseobacterium* strain Y35 exhibited inhibitory activity under all conditions, which was marginally enhanced by mangiferin (0.4 mmol L^{-1}) (Fig. 5C). In the case of *Chryseobacterium* strain Y14, its inhibitory capacity was promoted by L-tryptophan (2 mmol L^{-1}), acetoxyacetic acid (0.4 mmol L^{-1}), methoxyindoleacetic acid (0.4 mmol L^{-1}), O-phosphorylethanolamine (10 mmol L^{-1}), and mangiferin (0.4 mmol L^{-1}). And there was a potential link between L-tryptophan (2 mmol L^{-1})-triggered inhibition and the growth promotion of Y14 induced by the same compound (Fig. 5C and Table S11). *Paenibacillus* strain R16 exhibited inhibitory effects under treatment with L-tryptophan (0.4 mmol L^{-1}, 2 mmol L^{-1}, and 10 mmol L^{-1}), methoxyindoleacetic acid (0.4 mmol L^{-1}), and O-phosphorylethanolamine (10 mmol L^{-1}) treatment (Fig. 5C). The stimulatory effect of *Dyadobacter* strain Y33 on *R. solanacearum* shifted to inhibitory when supplemented with methoxyindoleacetic acid (0.4 mmol L^{-1}) (Fig. 5C). All statistical test results are provided in Tables S12 to 23.

Discussion

It is widely recognized that the control of soil-borne disease is closely linked to soil nutrient properties [42]. In the current study, we investigated the influence of phosphorus availability on soil disease suppression. Using a 6-year continuous field trial of tomato with four different fertilization treatments, we identified soil available phosphorus as an important factor contributing to the control of bacterial wilt caused by soil-borne pathogen *R.*
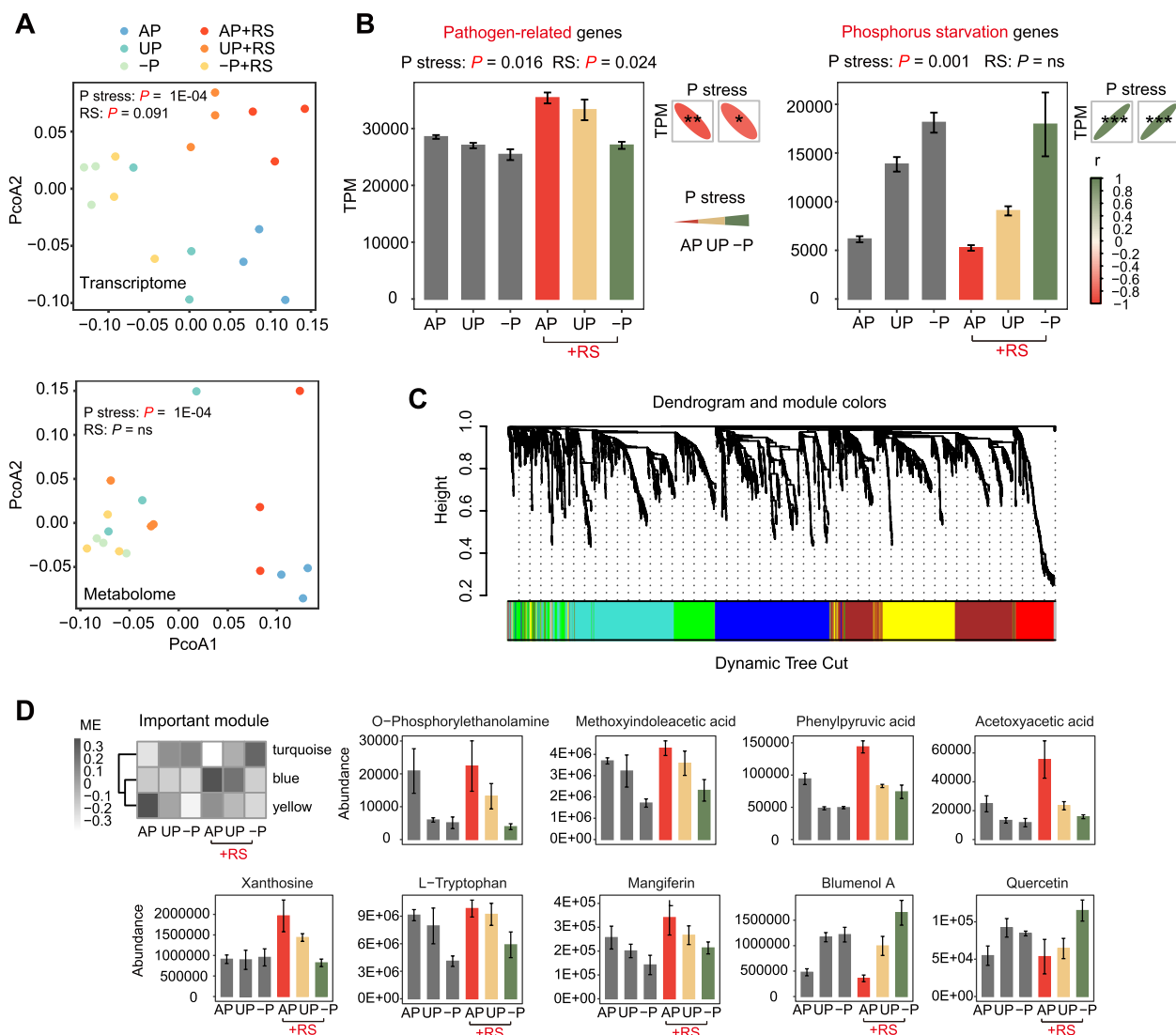
Fig. 4 Impact of phosphorus and pathogen inoculation on plant transcriptome and metabolome. Phosphorus stress gradually increased in the order of AP, UP, and −P due to different fertilizer treatments. The +RS groups indicated treatments inoculated with the pathogen. **A** PCoA plot illustrating the distance of the plant transcriptome and metabolome in different treatments. PERMANOVA test evaluated differences due to pathogen inoculation, while the Mantel test assessed the effect of the phosphorus gradient. **B** The transcripts per million (TPM) of pathogen-related genes and phosphorus starvation genes in different treatments and their correlations with phosphorus stress. Error bars represent standard errors with three replicates. Significance was determined using the Scheirer-Ray-Hare test and Spearman correlations. **C** Weighted gene co-expression network analysis (WGCNA) network of pathogen-related genes, phosphorus starvation genes, and all root metabolites. Members with similar trends were clustered and further divided into several modules with a minimum member size of 200, which were represented by the colors below. **D** Dendrogram depicting the key module eigengenes (ME) affected by phosphorus stress and pathogen inoculation. The histogram showing the abundances of key metabolites in the corresponding modules. Error bars represent standard errors with three replicates. "r" stands for Spearman correlation coefficient; *P* denotes phosphorus. Significance levels are denoted as follows: "ns," not significant, "'"$P < 0.1$, "*"$P < 0.05$, "**"$P < 0.01$, and "***"$P < 0.001$

solanacearum. We then conducted series of pot experiments to examine this phenomenon in more detail. Results showed that phosphorus adequacy increased the disease-suppressive potential of rhizosphere microbiome, while phosphorus deficiency increased this potential in the bulk soil. Furthermore, we found that plant

selection for specific microorganism in rhizosphere was a key driver of this observed discrepancy, resulting from a trade-off between defense function and phosphorus acquisition in plants (Fig. 6).

Phosphorus is a vital macronutrient involved in numerous biological functions [43]. However, phosphorus, in
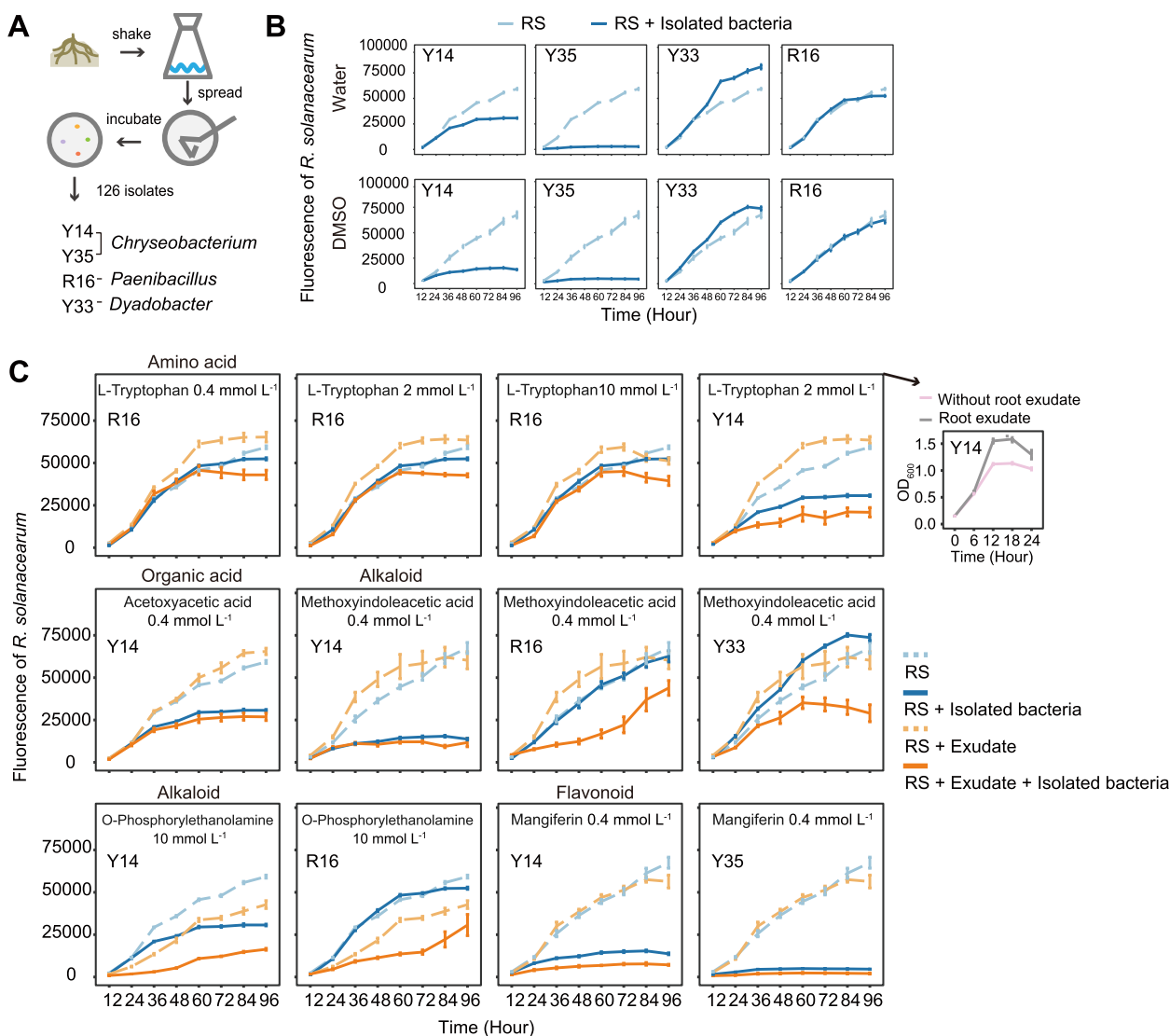
Fig. 5 Plant root exudates enhance the inhibitory capability of key isolated microbial taxa in the rhizosphere against the pathogen *R. solanacearum*. **A** Schematic of the isolation experiment. Key bacteria Y14, Y35, Y33, and R16 were selected for further experimentation. These four isolates, along with the root exudates used in subsequent experiments, were all promoted by improved phosphorus availability. **B** Growth of the pathogen *R. solanacearum* was quantified by measuring fluorescence intensity in the presence or absence of the key bacterial isolates. Water or dimethyl sulfoxide (DMSO) was added to the system as a control group for root exudates soluble in water or DMSO, respectively. **C** Growth of the pathogen *R. solanacearum* was quantified by measuring fluorescence intensity in the presence or absence of the key bacterial isolates and supplementation with key root exudates detected in our pot experiment. Additionally, the growth of strain Y14 when supplemented with L-tryptophan at a concentration of 2 mmol L^{-1} is provided (small inset plot, right). Significance was determined using the Scheirer-Ray-Hare test, as described in the supplementary materials. Error bars represent standard deviations with six replicates. RS denotes *R. solanacearum*. OD_{600} denotes absorbance value at a wavelength of 600 nm

the form of plant-available orthophosphate, is typically difficult to acquire due to its extremely slow diffusion and strong binding to metals or recalcitrant organophosphates in soil [44]. Thus, the critical function and general limitation of phosphorus significantly affect the behaviors of both plants and soil microorganisms [45, 46], and it was therefore not surprising that soil available phosphorus

proved to be more important than other nutrients in our field trial with respect to determining the level of disease incidence. To investigate the impact of phosphorus availability on soil disease suppression, we performed a pot experiment using NRPS, PKS related, and *hcnAB* functional genes to evaluate the soil microbiome's disease-suppressive potential under varying phosphorus levels.
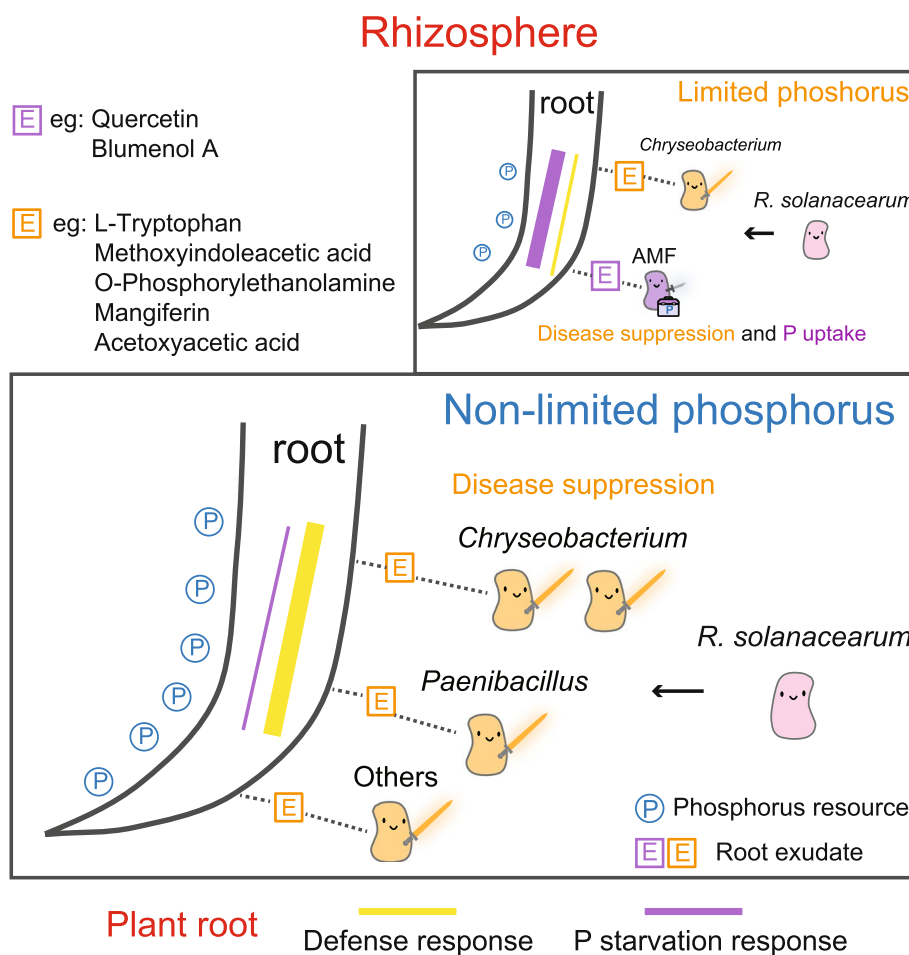
Rhizosphere

Fig. 6 A schematic model summarizing the effects of phosphorus on disease-suppressive function of soil microbiome in the rhizosphere through plant-microbe interactions. Available phosphorus resource is represented by blue circles with "P" in them. Squares with "E" represent various root exudates. Pink pawns represent the soil-borne pathogen *R. solanacearum*. Yellow pawns represent biocontrol microorganisms recruited by the plant root. Purple pawn represents AMF which contribute to both disease resistance and phosphorus acquisition. The yellow or purple lines in the root represent the defense or phosphorus starvation responses in tomato plants

The experiment included treatments both with and without pathogen inoculation. Interestingly, the alleviation of phosphorus stress promoted the disease-suppressive function in the rhizosphere, while the opposite response was found in bulk soil. This finding highlights the importance of the rhizosphere as a soil zone in which the microbiome, as influenced by the plant, plays a key role in disease suppression. We further identified several disease-suppressive taxa that were increased by improved phosphorus availability, including *Chryseobacterium*, *Dyadobacter* (phylum Bacteroidetes), *Rhizobium*, *Variovorax*, and *Hyphomicrobium* (phylum Proteobacteria) and *Paenibacillus* (phylum Firmicutes), with *Chryseobacterium* to be the most important taxon. These taxa exhibited similar trends to the disease-suppressive genes of the soil microbiome in the rhizosphere. *Chryseobacterium* species are known as effective biocontrol agents against

soil-borne pathogens, producing antifungal proteases and HCN [47, 48]. Their population density in the rhizosphere even predicts disease outcomes in tomato plants infected with *R. solanacearum* [49]. In addition, *Paenibacillus* has been widely reported to help plants defend against a broad spectrum of pathogens through its antimicrobial activity [50], while *Dyadobacter's* role in disease suppression is lesser known, despite one report linking it to *Fusarium* wilt suppression [51].

Given the opposite trends observed between bulk soil and rhizosphere, we aimed to uncover the driving force behind. We hypothesized that plant selection is pivotal, as plants actively shape their rhizosphere microbiome, recruiting microorganisms to combat pathogens [52, 53]. Our transcriptome analysis supports this notion. Tomato roots experiencing phosphorus deficiency exhibited a heightened response of phosphorus

starvation but suppressed response to pathogen inoculation. Notably, this defense function of plants exhibited a trend very similar to the disease-suppressive function of rhizosphere microbiome. This trade-off suggests prioritization of phosphate acquisition over defense under phosphorus limitation. Consistently, prior research demonstrates that master transcriptional regulators in phosphate stress response directly inhibit plant defense in *Arabidopsis thaliana* [6]. Foliar phosphite application suppresses the phosphate starvation response and activates plant defense under low phosphate conditions in tomato [54]. Thus, reduced defense investment under phosphorus deficiency presumably results in less investment in recruitment of biocontrol microorganisms in the rhizosphere. Similarly, plant immunity was reported to be suppressed through the PHR1-RALF-FERONIA pathway to alleviate phosphate starvation by shaping the root relevant microbiome, again highlighting the effects of the plant trade-offs in associated microbiome [55]. Additionally, this trade-off may be bidirectional. When we increased the pathogen pressure via pathogen inoculation, transcriptomic patterns shifted in the plants experiencing moderate phosphorus stress, with a general downregulation of phosphorus starvation genes and an upregulation of genes involved in defense mechanisms. This indicates that plants employ a sophisticated strategy to optimize investment in defense versus phosphorus acquisition. Thus, patterns of rhizosphere microbiome recruitment by the plant can be seen as an extension of plant responses to increased phosphorus supply. This underscores plant selection's role in altering disease-suppressive microbes, reversing the bulk soil trends.

We further sought to examine the mechanisms by which plants can improve their defense via the rhizosphere microbiome upon increased phosphorous availability. We specifically looked at the importance of root exudates as drivers of microbiome recruitment. In our study, we identified microbial populations and specific root exudates that were promoted by increased phosphorus supply and subsequently examined their interactions with the pathogen *R. solanacearum* via co-culture experiments. Results showed certain root exudates enhancing pathogen-inhibitory capacity of identified microbes. For instance, L-tryptophan, methoxyindoleacetic acid, O-phosphorylethanolamine, mangiferin, and acetoxyacetic acid boosted the pathogen inhibitory capacity of *Chryseobacterium*, which was reported to exhibit swarming activity [48] and engage in intense competition for root exudates during the biocontrol of *R. solanacearum* wilt [39]. Additionally, exposure to methoxyindoleacetic acid, O-phosphorylethanolamine, and L-tryptophan induced inhibitory effects on the pathogen by *Paenibacillus* R16

or *Dyadobacter* Y33. Moreover, previous results have shown that certain organic acids and flavonoids like mangiferin [56] can boost plant immunity by modulating plant-microorganism interactions in rhizosphere [57, 58]. Notably, Bacteroidetes, to which *Chryseobacterium* and *Dyadobacter* belong, have been reported to utilize phosphorylated compounds as carbon and energy sources, providing a competitive advantage when inhabiting zones of high microbial activity and nutrient demand [59]. In summary, certain root metabolites can improve control of the pathogen by recruiting disease-suppressive microbes, and improved soil phosphorus nutrient status facilitates this process.

Moreover, phosphorus-starved plants, despite a weakened disease-suppressive function in rhizosphere, can form symbiosis with arbuscular mycorrhizal fungi (AMF) in response to pathogen inoculation [60, 61], serving not only for defense but also for phosphorus acquisition [62, 63]. Similar to this strategy, previous studies have shown that plants favor relationships with ectomycorrhizal fungi under phosphorus deficiency. While this choice may result in lower phosphorus acquisition efficiency, it contributes more significantly to plant defense compared to alternative options [4, 64]. Our study indicates an AMF-based strategy for disease suppression is a favorable choice, and this symbiosis is further supported by the presence of key root exudates such as blumenol A and quercetin [65–67].

Our results were obtained under controlled conditions with consistent pathogen inoculation, which is different from field conditions. While phosphorus supply promotes plant defense and soil disease suppression in the rhizosphere, it may also promote pathogen proliferation in bulk soil, consequently heightening the risk of future infections. It remains to be seen to what extent this disparity of pathogen control between bulk and rhizosphere soils impacts the dynamics of disease incidence over time in the field. Future research should explore the optimal phosphorus levels for disease control and agricultural output, balancing benefits with the risks of excessive phosphorus.

Conclusions

Our 6-year field trial highlighted phosphorus availability as the primary factor influencing the control of tomato bacterial wilt by *R. solanacearum*. Pot experiments confirmed that adequate phosphorus activates plant immunity, improving rhizosphere microbiome function related to disease suppression, but not in the bulk soil. Adequate available phosphorus in the rhizosphere alleviates the trade-off between defense function and phosphorus acquisition in plants, promoting the production of root exudates, such as L-tryptophan and

O-phosphorylethanolamine, which enhance key microbial groups, such as *Chryseobacterium*, and their disease suppression capabilities in the rhizosphere. Plant selection emerges as the driver of the discrepancy between effects in bulk versus rhizosphere soil. In total, our study provides novel insights into the influence of phosphorus availability on the disease-suppressive functions of the rhizosphere microbiome. Understanding of how plant trade-offs between defense and phosphorous acquisition impact microbiome recruitment and function will help inform future strategies to optimize plant nutrition and natural biological control of plant pathogens.

Abbreviations

ITS	Internal transcribed spacer
NRPS	Nonribosomal peptide synthases
PKS	Polyketide synthases
CFU	Colony-forming units
NB	Nutrient Broth
zOTU	Zero-radius operational taxonomic units
TPM	Transcripts per million
OD	Optical density
PCoA	Principal coordinates analysis
WGCNA	Weighted gene co-expression network analysis
ME	Module eigengenes
DI	Disease incidence
AVP	Available phosphorus
SOM	Soil organic matter
DMSO	Dimethyl sulfoxide

Supplementary Information

Supplementary Material 1: Fig. S1. Information of field trial. (A) Overview of soil nutrient properties and disease incidence over the course of the continuous six-year trial. (B) Results of unary linear regression analysis depicting the relationship between soil organic matter, total nitrogen, available potassium contents and disease incidence. Fig. S2. Information of pot experiment. (A) Line graph displaying soil available phosphorus levels in different treatments during seasons 1 and 2, with error bars representing standard deviations. The results of significance test were in Supplementary Table 3. (B) The violin plot illustrating the fold change of the pathogen *Ralstonia solanacearum* in bulk and rhizosphere soils compared to the CK group. Scheirer Ray Hare tests were conducted. Fig. S3. Detailed results of individual genes related to disease suppression. The boxplot depicting the fold change of disease-resistant genes NRPS, PKS, and *hcnAB* compared to the CK group in bulk soil (top row) and rhizosphere soil (bottom row). + RS denotes *R. solanacearum* inoculation. Fig. S4. Shannon diversity of soil microbiome and microbial zOTUs responding to phosphorus stress. (A and B) Boxplot showing the Shannon diversity of soil microbial community in different treatments. Kruskal wallis test was conducted for the significance here. Manhattan plot showing the bacterial and fungal zOTUs significantly correlated with phosphorus stress (Spearman correlation, $P < 0.05$) in both bulk and rhizosphere soils. Fig. S5. Microbial taxa responding to phosphorus stress in bulk soil. (A) Butterfly plot illustrating bacterial zOTUs significantly correlated to phosphorus stress (Spearman correlation, $P < 0.05$). (B) Butterfly plot illustrating fungal zOTUs significantly correlated to phosphorus stress (Spearman correlation, $P < 0.05$). The numbers next to the histograms indicate the number of zOTUs in the corresponding genus. The "r" represents the correlation coefficient. Fig. S6. Bacterial taxa responding to phosphorus stress and pathogen inoculation in rhizosphere. (A) Cladogram displaying bacterial zOTUs negatively correlated to phosphorus stress pooled at the genus level in the rhizosphere (Spearman correlation, $P < 0.05$, each genus with

at least 6 or more zOTUs). (B) Cladogram displaying bacterial zOTUs positively correlated to phosphorus stress pooled at the genus level in the rhizosphere (Spearman correlation, $P < 0.05$, each genus with at least 6 or more zOTUs). The red and black triangles represent microbial taxa enriched or decreased by pathogen inoculation in the –P, UP, or AP groups using the Wilcoxon Test ($P < 0.05$). The "nelogp" denotes the negative log-transformed *P*-value of the Spearman correlations between the microbial taxa and phosphorus stress. "RA" stands for relative abundance. The classification (g: genus and phylum) is labelled behind the cladogram. Fig. S7. Fungal taxa responding to phosphorus stress and pathogen inoculation in rhizosphere. (A) Cladogram displaying fungal zOTUs negatively correlated to phosphorus stress pooled at the genus level in the rhizosphere (Spearman correlation, $P < 0.05$, each phylum with at least 6 or more zOTUs). (B) Cladogram displaying fungal zOTUs positively correlated to phosphorus stress pooled at the genus level in the rhizosphere (Spearman correlation, $P < 0.05$, each phylum with at least 6 or more zOTUs). The red and black triangles represent microbial taxa enriched or decreased by pathogen inoculation in the –P, UP, or AP groups using the Wilcoxon Test ($P < 0.05$). The "nelogp" denotes the negative log-transformed *P*-value of the Spearman correlations between the microbial taxa and phosphorus stress. "RA" stands for relative abundance. The classification (c: class, o: order, f: family, g: genus and phylum) is labelled behind the cladogram. Fig. S8. Phylogenetic relationship and morphology of the isolated key bacteria Y14 and Y35. Phylogenetic tree depicting the relationships between Y14 and Y35, isolated from rhizosphere soil, and key identified *Chryseobacterium* zOTUs. Images display the morphology of Y14 and Y35 after culturing for 3 or 14 days. The tree was generated using MEGA 11. Fig. S9. Phylogenetic relationship and morphology of the isolated key bacteria Y33. Phylogenetic tree depicting the relationships between Y33, isolated from rhizosphere soil, and key identified *Dyadobactor* zOTUs. Images display the morphology of Y33 after culturing for 3 or 14 days. The tree was generated using MEGA 11. Fig. S10. Phylogenetic relationship and morphology of the isolated key bacteria R16. Phylogenetic tree depicting the relationships between R16, isolated from rhizosphere soil, and key identified *Paenibacillus* zOTUs. Images display the morphology of R16 after culturing for 3 or 14 days. The tree was generated using MEGA 11. Fig. S11. Phylogenetic relationship and morphology of the 8 *Chryseobacterium* isolates. Phylogenetic tree depicting the relationships between the 8 *Chryseobacterium* isolates from rhizosphere soil. Images display the morphology of these isolates. The tree was generated using MEGA 11. Fig. S12. Relative abundances of the zOTUs that are most related to the isolated key bacteria. The zOTU1472 was most related to the isolated *Chryseobacterium* Y14; The zOTU13507 was most related to the isolated *Chryseobacterium* Y35; The zOTU11626 was most related to the isolated *Paenibacillus* R16; The zOTU13652 was most related to the isolated *Dyadobacter* Y33. Fig. S13. The influence of root exudate L-tryptophan on the inhibitory capability of key isolated microbial taxa against the pathogen. Line graph displaying the fluorescence intensity of pathogen affected by the key bacteria and L-tryptophan. Additional line graph plotting the OD_{600} of key bacteria influenced by L-Tryptophan. RS denotes *Ralstonia solanacearum*. OD_{600} is the absorbance at a wavelength of 600 nm. Fig. S14. The influence of root exudate O-phosphorylethanolamine on the inhibitory capability of key isolated microbial taxa against the pathogen. Line graph displaying the fluorescence intensity of pathogen affected by the key bacteria and O-phosphorylethanolamine. Additional line graph plotting the OD_{600} of key bacteria influenced by O-phosphorylethanolamine. RS denotes *Ralstonia solanacearum*. OD_{600} is the absorbance at a wavelength of 600 nm. Fig. S15. The influence of root exudate acetoxyacetic acid on the inhibitory capability of key isolated microbial taxa against the pathogen. Line graph displaying the fluorescence intensity of pathogen affected by the key bacteria and acetoxyacetic acid. Additional line graph plotting the OD_{600} of key bacteria influenced by acetoxyacetic acid. RS denotes *Ralstonia solanacearum*. OD_{600} is the absorbance at a wavelength of 600 nm. Fig. S16. The influence of root exudate methoxyindoleacetic acid on the inhibitory capability of key isolated microbial taxa against the pathogen. Line graph displaying the fluorescence intensity of pathogen affected by the key bacteria and methoxyindoleacetic acid. Additional line graph plotting the OD_{600} of key bacteria influenced by methoxyindoleacetic acid. RS denotes *Ralstonia solanacearum*. OD_{600} is the absorbance at a

wavelength of 600 nm. Fig. S17. The influence of root exudate phenylpyruvic acid on the inhibitory capability of key isolated microbial taxa against the pathogen. Line graph displaying the fluorescence intensity of pathogen affected by the key bacteria and phenylpyruvic acid. Additional line graph plotting the OD_{600} of key bacteria influenced by phenylpyruvic acid. RS denotes *Ralstonia solanacearum*. OD_{600} is the absorbance at a wavelength of 600 nm. Fig. S18. The influence of root exudate xanthosine on the inhibitory capability of key isolated microbial taxa against the pathogen. Line graph displaying the fluorescence intensity of pathogen affected by the key bacteria and xanthosine. Additional line graph plotting the OD_{600} of key bacteria influenced by xanthosine. RS denotes *Ralstonia solanacearum*. OD_{600} is the absorbance at a wavelength of 600 nm. Fig. S19. The influence of root exudate mangiferin on the inhibitory capability of key isolated microbial taxa against the pathogen. Line graph displaying the fluorescence intensity of pathogen affected by the key bacteria and mangiferin. Additional line graph plotting the OD_{600} of key bacteria influenced by mangiferin. RS denotes *Ralstonia solanacearum*. OD_{600} is the absorbance at a wavelength of 600 nm.

Supplementary Material 2: Table S1. Design of fertilization and pathogen inoculation in all treatments. Table S2. Primer sets in quantitative PCR experiment. Table S3. Primer sets in amplicon sequencing. Table S4. Soil nutrient properties during the pot experiment. Table S5. Identified bacteria isolates in rhizosphere (Similarty > = 97%). Table S6. Detailed information of individual bacterial zOTUs in Fig. 3. Table S7. Detailed information about pathogen-related genes in plant root. Table S8. Detailed information about phosphorus starvation genes in plant root. Table S9. Detailed information about key metabolites. Table S10. Significance test of co-culture experiment (referring to Fig. 5B). Table S11. Significance test of culture experiment (L-Tryptophan of 2 mmol L^{-1} on Y14). Table S12. Significance test of co-culture experiment (L-Tryptophan of 0.4 mmol L-1 on R16). Table S13. Significance test of co-culture experiment (L-Tryptophan of 2 mmol L-1 on R16). Table S14. Significance test of co-culture experiment (L-Tryptophan of 10 mmol L-1 on R16). Table S15. Significance test of co-culture experiment (L-Tryptophan of 2 mmol L-1 on Y14). Table S16. Significance test of co-culture experiment (Acetoxyacetic acid of 0.4 mmol L-1 on Y14). Table S17. Significance test of co-culture experiment (Methoxyindoleacetic acid of 0.4 mmol L-1 on Y14). Table S18. Significance test of co-culture experiment (Methoxyindoleacetic acid of 0.4 mmol L-1 on R16). Table S19. Significance test of co-culture experiment (Methoxyindoleacetic acid of 0.4 mmol L-1 on Y33). Table S20. Significance test of co-culture experiment (O-Phosphorylethanolamine of 10 mmol L-1 on Y14). Table S21. Significance test of co-culture experiment (O-Phosphorylethanolamine of 10 mmol L-1 on R16). Table S22. Significance test of co-culture experiment (Mangiferin of 0.4 mmol L-1 on Y14). Table S23. Significance test of co-culture experiment (Mangiferin of 0.4 mmol L-1 on Y35).

Acknowledgements

Authors' contributions

Funding

Availability of data and materials
Raw amplicon sequencing data was deposited at the National Center for Biotechnology Information (NCBI) under the accession number of PRJNA979018, PRJNA978981 and PRJNA1077633.

Declarations

Ethics approval and consent to participate
Not applicable.

Consent for publication
Not applicable.

Competing interests
The authors declare no competing interests

Author details
[1]The Sanya Institute of the Nanjing Agricultural University, Key Lab of Organic-Based Fertilizers of China, Jiangsu Provincial Key Lab for Solid Organic Waste Utilization, Jiangsu Collaborative Innovation Center of Solid Organic Wastes, Educational Ministry Engineering Center of Resource-Saving Fertilizers, Nanjing Agricultural University, Nanjing, Jiangsu 210095, China. [2]Wheat Health, Genetics and Quality Research Unit, Washington State University, Pullman, WA 99164, USA. [3]Molecular Microbiology, School of Biosciences, University of Sheffield, Sheffield S10 2TN, UK. [4]Ecology and Biodiversity Group, Department of Biology, Institute of Environmental Biology, Utrecht University, Padualaan 8, Utrecht 3584 CH, the Netherlands.

References

1. Saunders DGO. Will yield gains be lost to disease? Nat Clim Chang. 2021;11:648–9.
2. Janvier C, Villeneuve F, Alabouvette C, Edel-Hermann V, Mateille T, Steinberg C. Soil health through soil disease suppression: which strategy from descriptors to indicators? Soil Biol Biochem. 2007;39:1–23.
3. Berg M, Koskella B. Nutrient- and dose-dependent microbiome-mediated protection against a plant pathogen. Curr Biol. 2018;28:2487–92.
4. Laliberté E, Lambers H, Burgess TI, Wright SJ. Phosphorus limitation, soil-borne pathogens and the coexistence of plant species in hyperdiverse forests and shrublands. New Phytol. 2015;206:507–21.
5. Shen J, Yuan L, Zhang J, Li H, Bai Z, Chen X, et al. Phosphorus dynamics: from soil to plant. Plant Physiol. 2011;156:997–1005.
6. Castrillo G, Teixeira PJPL, Paredes SH, Law TF, de Lorenzo L, Feltcher ME, et al. Root microbiota drive direct integration of phosphate stress and immunity. Nature. 2017;543:513–8.
7. Cha JY, Han S, Hong HJ, Cho H, Kim D, Kwon Y, et al. Microbial and biochemical basis of a *Fusarium* wilt-suppressive soil. ISME J. 2016;10(1):119–29.
8. Teixeira PJP, Colaianni NR, Fitzpatrick CR, Dangl JL. Beyond pathogens: microbiota interactions with the plant immune system. Curr Opin Microbiol. 2019;49:7–17.
9. Kwak MJ, Kong HG, Choi K, Kwon SK, Song JY, Lee J, et al. Rhizosphere microbiome structure alters to enable wilt resistance in tomato. Nat Biotechnol. 2018;36:1100–9.
10. Carrión VJ, Perez-Jaramillo J, Cordovez V, Tracanna V, de Hollander M, Ruiz-Buck D, et al. Pathogen-induced activation of disease-suppressive functions in the endophytic root microbiome. Science. 2019;366:606–12.
11. Pieterse CM, de Jonge R, Berendsen RL. The soil-borne supremacy. Trends Plant Sci. 2016;21:171–3.
12. Zhou X, Guo Z, Chen C, Jia Z. Soil microbial community structure and diversity are largely influenced by soil pH and nutrient quality in 78-year-old tree plantations. Biogeosciences. 2017;14:2101–11.
13. Mendes R, Garbeva P, Raaijmakers JM. The rhizosphere microbiome: significance of plant beneficial, plant pathogenic, and human pathogenic microorganisms. FEMS Microbiol. 2013;37:634–63.
14. Chaparro JM, Sheflin AM, Manter DK, Vivanco JM. Manipulating the soil microbiome to increase soil health and plant fertility. Biol Fertil Soils. 2012;48:489–99.
15. Shen Z, Ruan Y, Xue C, Zhong S, Li R, Shen Q. Soils naturally suppressive to banana *Fusarium* wilt disease harbor unique bacterial communities. Plant Soil. 2015;393:21–33.

16. Li P, Liu M, Li G, Liu K, Liu T, Wu M, et al. Phosphorus availability increases pathobiome abundance and invasion of rhizosphere microbial networks by *Ralstonia*. Environ Microbiol. 2021;23:5992–6003.
17. Allen C, Prior P, Hayward AC. Bacterial wilt disease and the *Ralstonia solanacearum* species complex. St. Paul: APS Press; 2005.
18. Raaijmakers JM, De Bruijn I, Nybroe O, Ongena M. Natural functions of lipopeptides from *Bacillus* and *Pseudomonas*: more than surfactants and antibiotics. FEMS Microbiol Rev. 2010;34:1037–62.
19. Prieto C. Characterization of nonribosomal peptide synthetases with NRPSsp. Methods Mol Biol. 2016;1401:273–8.
20. Mendes R, Kruijt M, de Bruijn I, Dekkers E, van der Voort M, Schneider JHM, et al. Deciphering the rhizosphere microbiome for disease-suppressive bacteria. Science. 2011;332:1097–100.
21. Dudenhöffer JH, Scheu S, Jousset A. Systemic enrichment of antifungal traits in the rhizosphere microbiome after pathogen attack. J Ecol. 2016;104:1566–75.
22. Le TH, Sivachidambaram V, Yi X, Li X, Zhou Z. Quantification of polyketide synthase genes in tropical urban soils using real-time PCR. J Microbiol Methods. 2014;106:135–42.
23. Charlop-Powers Z, Owen JG, Reddy BVB, Ternei MA, Brady SF. Chemical-biogeographic survey of secondary metabolism in soil. PNAS. 2014;111:3757–62.
24. Borsetto C, Amos GC, da Rocha UN, Mitchell AL, Finn RD, Laidi RF, et al. Microbial community drivers of PK/NRP gene diversity in selected global soils. Microbiome. 2019;7:1–11.
25. Zhou T, Chen D, Li C, Sun Q, Li L, Liu F, et al. Isolation and characterization of *Pseudomonas brassicacearum* J12 as an antagonist against *Ralstonia solanacearum* and identification of its antimicrobial components. Microbiol Res. 2012;167:388–94.
26. Wang X, Wei Z, Yang K, Wang J, Jousset A, Xu Y, et al. Phage combination therapies for bacterial wilt disease in tomato. Nat Biotechnol. 2019;37:1513–20.
27. Schonfeld J, Heuer H, Van Elsas JD, Smalla K. Specific and sensitive detection of *Ralstonia solanacearum* in soil on the basis of PCR amplification of *fliC* fragments. Appl Environ Microbiol. 2003;69:7248–56.
28. Zhao M, Yuan J, Zhang R, Dong M, Deng X, Zhu C, et al. Microflora that harbor the NRPS gene are responsible for *Fusarium* wilt disease-suppressive soil. Appl Soil Ecol. 2018;132:83–90.
29. Yuan J, Zhao M, Li R, Huang Q, Rensing C, Raza W, et al. Antibacterial compounds-macrolactin alters the soil bacterial community and abundance of the gene encoding PKS. Front Microbiol. 2016;7:1904.
30. Zheng B, Zhu Y, Sardans J, Peñuelas J, Su J. QMEC: a tool for high-throughput quantitative assessment of microbial functional potential in C, N, P, and S biogeochemical cycling. Sci China Life Sci. 2018;61:1451–62.
31. Khan-Malek R, Wang Y. Drug safety evaluation: methods and protocols: statistical analysis of quantitative RT-PCR results. Passaic County: Humana Press; 2017.
32. Martin M. Cutadapt removes adapter sequences from high-throughput sequencing reads. EMBnet J. 2011;17:10–2.
33. Edgar RC. UNOISE2: improved error-correction for Illumina 16S and ITS amplicon sequencing. BioRxiv. 2016;081257.
34. Edgar RC. SINTAX: a simple non-Bayesian taxonomy classifier for 16S and ITS sequences. Biorxiv. 2016;074161.
35. Shen Z, Penton CR, Lv N, Xue C, Yuan X, Ruan Y, et al. Banana *Fusarium* wilt disease incidence is influenced by shifts of soil microbial communities under different monoculture spans. Microb Ecol. 2018;75:739–50.
36. Bao S. Soil agricultural chemistry analysis. Beijing: China Agriculture Press; 2013.
37. Nishioka T, Elsharkawy MM, Suga H, Kageyama K, Hyakumachi M, Shimizu M. Development of culture medium for the isolation of *Flavobacterium* and *Chryseobacterium* from rhizosphere soil. Microbes Environ. 2016;31:104–10.
38. Frank JA, Reich CI, Sharma S, Weisbaum JS, Wilson BA, Olsen GJ. Critical evaluation of two primers commonly used for amplification of bacterial 16S rRNA genes. Appl Environ Microbiol. 2008;74:2461–70.
39. Huang J, Wei Z, Hu J, Yang C, Gu Y, Mei X, et al. *Chryseobacterium nankingense* sp. Nov. WR21 effectively suppresses *Ralstonia solanacearum* growth via intensive root exudates competition. BioControl. 2017;62:567–77.
40. Gu Y, Wei Z, Wang X, Friman VP, Huang J, Wang X, et al. Pathogen invasion indirectly changes the composition of soil microbiome via shifts in root exudation profile. Biol Fertil Soils. 2016;52:997–1005.
41. Gu Y, Hou Y, Huang D, Hao Z, Wang X, Wei Z, et al. Application of biochar reduces *Ralstonia solanacearum* infection via effects on pathogen chemotaxis, swarming motility, and root exudate adsorption. Plant Soil. 2017;415:269–81.
42. Dordas C. Role of nutrients in controlling plant diseases in sustainable agriculture A review. Agron Sustain Dev. 2008;28:33–46.
43. Péret B, Clément M, Nussaume L, Desnos T. Root developmental adaptation to phosphate starvation: better safe than sorry. Trends Plant Sci. 2011;16:442–50.
44. White PJ, Hammond JP. The ecophysiology of plant-phosphorus interactions: phosphorus nutrition of terrestrial plants. New York: Springer Science & Business Media; 2008.
45. Lidbury IDEA, Borsetto C, Murphy ARJ, Bottrill A, Jones AME, Bending GD, et al. Niche-adaptation in plant-associated Bacteroidetes favours specialisation in organic phosphorus mineralisation. ISME J. 2021;15:1040–55.
46. Lidbury IDEA, Murphy ARJ, Scanlan DJ, Bending GD, Jones AME, Moore JD, et al. Comparative genomic, proteomic and exoproteomic analyses of three *Pseudomonas* strains reveals novel insights into the phosphorus scavenging capabilities of soil bacteria. Environ Microbiol. 2016;18:3535–49.
47. Gandhi Pragash M, Narayanan KB, Naik PR, Sakthivel N. Characterization of *Chryseobacterium aquatium* strain PUPC1 producing a novel antifungal protease from rice rhizosphere soil. J Microbiol Biotechnol. 2009;19:99–107.
48. Kim H, Sang M, Jung H, Jeun Y, Myung I, Kim K. Identification and characterization of *Chryseobacterium wanjuense* strain KJ9C8 as a biocontrol agent of Phytophthora blight of pepper. Crop Prot. 2012;32:129–37.
49. Gu Y, Banerjee S, Dini-Andreote F, Xu Y, Shen Q, Jousset A, et al. Small changes in rhizosphere microbiome composition predict disease outcomes earlier than pathogen density variations. ISME J. 2022;16:2448–56.
50. Von der Weid I, Alviano DS, Santos ALS, Soares RMA, Alviano CS, Seldin L. Antimicrobial activity of *Paenibacillus peoriae* strain NRRL BD-62 against a broad spectrum of phytopathogenic bacteria and fungi. J Appl Microbiol. 2003;95:1143–51.
51. Fu L, Penton CR, Ruan Y, Shen Z, Xue C, Li R, et al. Inducing the rhizosphere microbiome by biofertilizer application to suppress banana *Fusarium* wilt disease. Soil Biol Biochem. 2017;104:39–48.
52. Berendsen RL, Pieterse CM, Bakker PA. The rhizosphere microbiome and plant health. Trends Plant Sci. 2012;17:478–86.
53. Ge A, Liang Z, Xiao J, Zhang Y, Zeng Q, Xiong C, et al. Microbial assembly and association network in watermelon rhizosphere after soil fumigation for *Fusarium* wilt control. Agric Ecosyst Environ. 2021;312:107336.
54. Viñas M, Mendez JC, Jiménez VM. Effect of foliar applications of phosphites on growth, nutritional status and defense responses in tomato plants. Sci Hortic. 2020;265:109200.
55. Tang J, Wu D, Li X, Wang L, Xu L, Zhang Y, et al. Plant immunity suppression via PHR1-RALF-FERONIA shapes the root microbiome to alleviate phosphate starvation. EMBO J. 2022;41:e109102.
56. Sudheeran PK, Sela N, Carmeli-Weissberg M, Ovadia R, Panda S, Feygenberg O, et al. Induced defense response in red mango fruit against *Colletotrichum gloeosporioides*. Hort Res. 2021;8:17.
57. Ghitti E, Rolli E, Crotti E, Borin S. Flavonoids are intra- and inter-kingdom modulator signals. Microorganisms. 2022;10:2479.
58. Wen T, Yuan J, He X, Lin Y, Huang Q, Shen Q. Enrichment of beneficial cucumber rhizosphere microbes mediated by organic acid secretion. Hort Res. 2020;7:154.
59. Lidbury IDEA, Scanlan DJ, Murphy ARJ, Christie-Oleza JA, Aguilo-Ferretjans MM, Hitchcock A, et al. A widely distributed phosphate-insensitive phosphatase presents a route for rapid organophosphorus remineralization in the biosphere. Proc Natl Acad Sci USA. 2022;119:e2118122119.
60. Qu L, Wang M, Biere A. Interactive effects of mycorrhizae, soil phosphorus, and light on growth and induction and priming of defense in Plantago lanceolata. Front Plant Sci. 2021;12:647372.
61. Gerlach N, Schmitz J, Polatajko A, Schlüter U, Fahnenstich H, Witt S, et al. An integrated functional approach to dissect systemic responses in maize to arbuscular mycorrhizal symbiosis. Plant Cell Environ. 2015;38(8):1591–612.
62. Weng W, Yan J, Zhou M, Yao X, Gao A, Ma C, et al. Roles of arbuscular mycorrhizal fungi as a biocontrol agent in the control of plant diseases. Microorganisms. 2022;10:1266.

63. Jeffries P, Gianinazzi S, Perotto S, Turnau K, Barea JM. The contribution of arbuscular mycorrhizal fungi in sustainable maintenance of plant health and soil fertility. Biol Fertil Soils. 2003;37:1–16.

64. Albornoz FE, Burgess TI, Lambers H, Etchells H, Laliberté E. Native soilborne pathogens equalize differences in competitive ability between plants of contrasting nutrient-acquisition strategies. J Ecol. 2017;105:549–57.

65. Wang M, Schäfer M, Li D, Halitschke R, Dong C, McGale E, et al. Blumenols as shoot markers of root symbiosis with arbuscular mycorrhizal fungi. Elife. 2018;7:e37093.

66. You Y, Ray R, Halitschke R, Baldwin G, Baldwin IT. AMF-indicative blumenol-C-glucosides predict lipid accumulations and fitness in plants grown without competitors. New Phytol. 2023;238:2159–74.

67. Campos-Lopez A, Uribe-Lopez JA, Cazares-Ordonez V, Garibay-Orijel R, Valdez-Cruz NA, Trujillo-Roldan MA. Quercetin and 1-methyl-2-oxindole mimic root signaling that promotes spore germination and mycelial growth of *Gigaspora margarita*. Mycorrhiza. 2022;32:177–91.

Publisher's Note